COMMUNICATIONS IN SCIENCE AND TECHNOLOGY
Homepage: cst.kipmi.or.id

Ytterbium-doped TeO_2-ZnO-Na_2O glasses: Insights into physical, mechanical, and optical properties

Devara Ega Fausta[a], Agus Supriyanto[a,*], Ahmad Marzuki[a], Fahru Nurosyid[a], Rachmat Hidayat[b] Saidatul Nisya[a], Kharenina Zalfa' Shalihah[a]

[a]*Department of Physics, Universitas Sebelas Maret, Surakarta 57216, Indonesia*
[b]*Department of Physics, Institut Teknologi Bandung, Bandung 40132, Indonesia*

Article history:
Received: 28 December 2025 / Received in revised form: 2 March 2026 / Accepted: 24 March 2026

Abstract

This present study constitutes a systematic investigation imto the influence of low-concentration Yb_2O_3 incorporation on the physical, mechanical, and optical properties of TeO_2 ZnO Na_2O (TZN) glasses. The glasses under consideration are composed of $65TeO_2$-(30-x)ZnO-$5Na_2O$- xYb_2O_3 (x = 0-2.5 mol%). The fabrication process utilized the conventional melt-quenching technique. The present study specifically addresses the limited understanding of how minor Yb^{3+} incorporation affects the structure-property relationships in TZN glass systems. The results obtained demonstrate progressive densification of the glass network in the presence of increasing Yb_2O_3 content. This is evidenced by an increase in density from 5.15 to 5.62 g cm^{-3} and a corresponding decrease in molar volume. This phenomenon is correlated to enhanced network connectivity and it was attributed to the alteration of Non-Bridging Oxygen (NBO) to Bridging Oxygen (BO) linkages. Consequently, an enhancement in mechanical properties is observed with increasing both Young's (50.67 to 52.61 GPa) and Bulk (29.77 to 31.89 GPa) modulus, respectively. It is suggested that these factors result in enhanced glass rigidity and durability. The optical investigation demonstrates a broadening of the optical band gap from 3.01 to 3.30 eV. This suggests the presence of a denser glass network and declined glass electronic polarizability. The findings of the study indicated that the integration of low-level Yb_2O_3 into TZN-based glasses can result in a modification of the glasses properties, thereby highlighting the potential for advanced application in the domain of photonics.

Keywords: Densification; elastical moduli; optical band gap; tellurite glass; Yb^{3+}doping

1. Introduction

Tellurite glasses have attracted noteworthy attention since their first report in 1952 due to their unique combination of properties. The properties of the material under consideration include low phonon energy (600-800 cm^{-1}), high solubility of rare-earth ions, a broad infrared transmission window, and relatively low melting temperatures approximately 700-900°C, in comparison with conventional silica and borate based glasses [1]. These characteristics render tellurite-based systems highly attractive as host materials for a wide range of optoelectronics applications, particularly in rare-earth doped devices such as solid-state lasers, optical amplifiers, and optical sensors [2]. However, pure TeO_2 exhibits substandard glass forming ability and a strong propensity to crystallize. To overcome this limitation, it is imperative to incorporate of suitable modifier oxides with the objective of suppressing crystallization, enhancing thermal stability, and stabilizing the glass network structure [3].

* Corresponding author.
Email: agusf22@staff.uns.ac.id
https://doi.org/10.21924/cst.11.1.2026.1869

A wide range of tellurite-based glass systems has been developed through the addition of various modifier oxides, including TeO_2-ZnO [4], TeO_2-WO_5 [5], TeO_2-ZnO-Li_2O (TZL) [6], TeO_2-ZnO-BaO (TZBa) [7], TeO_2- ZnO-PbO (TZPb) [8], TeO_2- ZnO- Bi_2O_3 (TZBi) [9], TeO_2- ZnO- B_2O_3 (TZB) [10] and TeO_2-ZnO-Na_2O (TZN) [11]. The structural, thermal, and optical properties of these systems are found to be cotingent on the nature and concentration. of the modifier oxides. Of these, the TZN glass system has received considerable attention due to its balanced glass-forming ability, relatively good thermal stability, and suitability as an efficient host matrix for rare-earth ion doping.

It has been demonstrated by previous studies that rare-earth doped TZN glasses for photonic application through detailed investigation of their structural, thermal, mechanical, spectroscopic, and luminescent properties. For instance, Ghosal et al. reported enhanced glass stability and twofold increase in upconversion luminescence in Er_2O_3-doped TZN-Ag glasses, highlighting their potential for solid-state laser and nanophotonic applications [12]. Badamasi and Tanko observed high thermal stability (exceeding 100°C) and favourable Hruby parameters in Dy_2O_3-TZN glasses, indicating their suitability

for fibre-drawing applications [13]. Voss et al. confirmed the amorphous nature of Eu_2O_3-doped TZN glasses despite synthesis challenges [14], while Mirdda et al. reported tunable optical properties, robust thermal stability, and stable dielectric performance in Nd_2O_3-doped TZN systems [15]. Furthermore, Shen et al. demonstrated that compositional substitution between ZnO and Na_2O in TZN-Tm_2O_3 glasses induces a red shift in the emission band near 1.47 μm, emphasizing the strong dependence of optical properties on modifier composition [16].

Among the rare earth ions, ytterbium oxide (Yb_2O_3) is of particular interest due to its simple two-level energy structure. Furthermore, it has been demonstrated to play pivotal role in the sensitization of photonic materials, as evidenced by numerous studies [17,18]. The incorporation of the subject into tellurite glass systems has been the subject of extensive research, which has demonstrated significant effects on the performance of optical and spectroscopic systems [19,20]. Nevertheless, despite extensive research on rare-earth doped TZN glasses, systematic studies focusing on the influence of low Yb_2O_3 concentrations on the coupled physical, mechanical, and spectroscopic properties of the TeO_2-ZnO-Na_2O system remain limited.

In this context, the present study investigates the effect of low-level Yb_2O_3 incorporation on the structural, physical, mechanical, and optical properties over the UV-Vis to infrared spectral range. Glasses with composition $65TeO_2$-(30-x)ZnO-$5Na_2O$- xYb_2O_3 (x = 0-2.5 mol%) were prepared via conventional melt-quenching technique and systematically characterized. This objective of this study is to establish clear structure-property correlations and to provide more profound of the role of Yb^{3+} ions in tailoring tellurite glass networks. This is with a view to supporting their potential application in advanced photonic and optoelectronic devices.

2. Materials and Methods

2.1. Fabrication

Glass samples with composition $65TeO_2$-(30-x)ZnO-$5Na_2O$- xYb_2O_3 (denoted as TZNYb), where x = 0, 0.5, 1.0, 1.5, 2.0, and 2.5 mol% were prepared using the conventional melt-quenching technique. The synthesis was carried out using raw materials of the highest purity, namely tellurium dioxide (TeO_2, 99.9%, Wuhan Xinrong), zinc oxide (ZnO, 99%, Loba Chemie), sodium carbonate (Na_2CO_3, 99.5%, Pallav) and ytterbium oxide (Yb_2O_3, 99.9%, Shanghai Ximeng). The batch compositions were determined using stoichiometric calculations for a total mass of approximately 10 g. The raw materials were accurately weighed using an analytical digital balance and thoroughly homogenized by grinding in a ceramic mortar with a pestle for 1 h to ensure compositional uniformity.

The homogenized mixture was transferred into an aluminum crucible and subsequently melted in an electric furnace at temperature 900°C for 30 minutes. A rectangular brass mould with dimension of 3.5x2.5x0.25 cm^3 was subjected to a preliminary heating process in a laboratory oven set at 250°C to minimize thermal shock during casting. The molten glass was then poured into the preheated mould and immediately transferred to an annealing furnace, where it was held at 285°C for 8 hours. This was followed by slow cooling to room temperature to relieve internal stresses.

The obtained glass samples were subsequently polished using silicon carbide abrasive papers. The finer grit sizes (1000, 1500, 2000, 3000, 4000, and 5000) were selected to acquire smooth and scratch-free surfaces for further characterization purpose.

2.2. Characterisation

The density of the glass samples was determined at room temperature using Archimedes principle with a pycnometer and distilled water as the immersion medium. The density (ρ_g) was calculated using the standard relation given in Eq. (1) [21]:

$$\rho_g = \left[\frac{(m_{g+p})-(m_p)\,\rho_d}{(m_{g+p}-m_p)-(m_{g+d+p}-m_{d+p})}\right] \quad (1)$$

where ρ_g and ρ_d denote the densities of the glass and distilled water, respectively; m_p is the mass of the empty pycnometer; m_{g+p} is the mass of pycnometer containing the glass sample; m_{d+p} is the mass of pycnometer filled with distilled water; and m_{g+d+p} represents the mass of pycnometer containing both glass and distilled water.

Derived physical parameters including molar volume (V_m), oxygen packing density (OPD), Yb^{3+} ion concentration (N_{Yb3+}), polaron radius (r_p), interionic distance (r_i), field strength (F_s), and packing density (V_p) were calculated using the Eq. (2) - (8) [22,23]:

$$V_m = \frac{\sum(n_i.X_i)}{\rho_g} \quad (2)$$

$$N_{Yb3+} = \frac{N_A\, n_{Yb3+}\, \rho_g}{M_w} \quad (3)$$

$$OPD = \left(\frac{O}{V_m}\right) 1000 \quad (4)$$

$$r_p = \frac{1}{2}\left(\frac{\pi}{6N_{Yb3+}}\right)^{\frac{1}{3}} \quad (5)$$

$$r_i = \left(\frac{1}{N_{Yb3+}}\right)^{\frac{1}{3}} \quad (6)$$

$$F_s = \frac{z}{r_{p^2}} \quad (7)$$

$$V_p = \frac{1}{V_m}\sum_i (V_i.x_i) \quad (8)$$

where n_i represents the molar fraction of each oxide component, x_i is the molecular weight, O denotes the total number of oxygen atoms in the glass network, N_A is Avogadro's number ($6{,}023\times10^{23}$ mol^{-1}), n_{Yb3+} is molar fraction of Yb_2O_3, Z is the valence of Yb^{3+} ions, and V_i represents the packing factor of each oxide component.

Fourier Transform Infrared (FTIR) spectra were recorded utilizing a Shimadzu IR Prestige-21 Spectrometer encompassing the wavenumbers range from 400 to 4000 cm^{-1} employing KBr pellet technique. All the measurements were performed at room temperature (≈25°C). The relative fraction of TeO_4 structural units (N_4) was estimated using Eq. (9) [24]:

$$N_4 = \frac{A_{TeO4}}{A_{TeO3} + A_{TeO4}} \quad (9)$$

where A_{TeO4} and A_{TeO3} correspond to the integrated areas of TeO_3 and TeO_4 units, respectively.

The Ultraviolet-Visible (UV-Vis) absorption spectra were recorded using a Ocean Optics DH-2000-BAL double-beam spectrophotometer over the wavelength range of 200-1100 nm. The absorption coefficient (α) was calculated from the measured absorbance (A) and sample thickness (d) using Eq. (10):

$$\alpha = 2.303 \frac{A}{d} \quad (10)$$

The optical band gap energy (E_g) was determined using the Tauc plot method based on the Davis-Mott model, assuming an indirect allowed transition (n=1/2), as expressed in Eq. (11) [25]:

$$(\alpha h\nu)^{1/2} = C\,(h\nu - E_g) \quad (11)$$

where α is absorption coefficient, $h\nu$ is the photon energy, and C is the proportional constant.

The subsequent optical parameters were calculated based on the obtained optical band gap: glass refractive index (n), molar refractivity (R_m), electronic molar polarisability (α_m), and reflection loss (R_L) were calculated using Eq. (12-15) [26] :

$$(n^2 - 1)/(n^2 + 2) = 1 - \sqrt{(E_g/20)} \quad (12)$$

$$R_L = \frac{n^2-1}{n^2+1} \quad (13)$$

$$R_m = \frac{(n^2-1)}{(n^2+1)} V_m \quad (14)$$

$$\alpha_m = \left(\frac{3}{4\pi N_A}\right) R_m \quad (15)$$

In addition, to Eq. (12), the refractive index was also estimated using empirical models proposed by Dimitrov-Sakka ($n_{D\text{-}S}$), Moss (n_M), and Kumar (n_R) as given in Eq. (16), (17), and (18), respectively:

$$n_{D-S} = \sqrt{\left(\frac{3}{E_g}\right)} - 2 \quad (16)$$

$$n_M = \sqrt[4]{\left(\frac{95}{E_g}\right)} \quad (17)$$

$$n_R = -0.73 \ln (0.0274\, E_g) + 0.5511 \quad (18)$$

The mechanical properties including the modulus Young's (E), Bulk (B), Shear (S), Longitudinal (L), Poisson ratio (σ), and Micro-hardness (H) were estimated using the Makishima-Mackenzie model, as expressed in Eq. (19-24) [27]:

$$E = 2\, V_p G \quad (19)$$

$$B = 1.2\, V_p E \quad (20)$$

$$S = \frac{3EB}{9B-E} \quad (21)$$

$$L = B + \frac{3}{4} S \quad (22)$$

$$\sigma = 0.5 - \frac{1}{7.2} V_p \quad (23)$$

$$H = \frac{(1-2\sigma)}{6\,(1+\sigma)} \quad (24)$$

3. Results and Discussion

3.1. Physical properties

The density of the TZN glass increases systematically from 5.15 g cm^{-3} to 5.62 g cm^{-3} with increasing Yb_2O_3 concentration, corresponding to an overall increase of approximately 9.12%. Conversely, the molar volume (V_m) exhibits a decline from 25.47 cm^3 to 24.75 cm^3, as demonstrated in Fig. 1**.** This inverse relationship is consistent with other previous reports [28]. The molar volume is determined by the mean average molecular weight and the density of the glass. In the present system, an increase in the average molecular weight is observed from 131.25 to 139.06 g mol^{-1}. This is attributable to the partial substitution of ZnO (81.38 g mol^{-1}) with significantly heavier Yb_2O_3 (394.08 g cm^{-1}), thereby reducing the V_m value [29]. Furthermore, an increase in Yb_2O_3 content is accompanied by an enhancement in packing density (V_p), which increases from 0.490 to 0.505. This phenomenon can be attributed to the higher ionic packing factor of Yb_2O_3 (Vi = 8.6 cm^3) compared to ZnO (Vi = 7.9 cm^3) [30]. It promotes a more efficiently packed glass network. A similar trend is observed in the examination of oxygen packing density (OPD), which increases from 64.76 to 68.69 mol L^{-1} as the total number of oxygen atoms rises from 165 to 170.

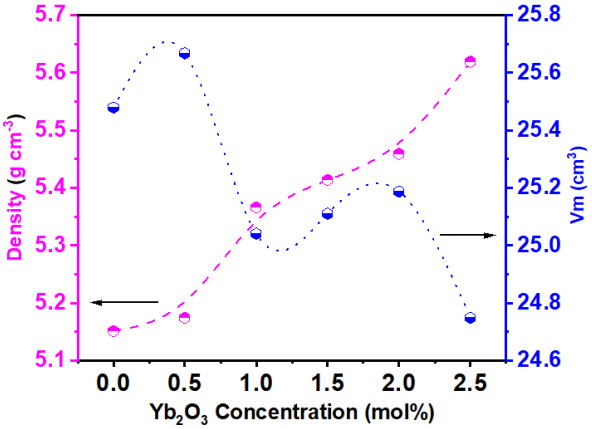

Fig. 1. Density and molar volume (V_m) as function of Yb_2O_3 concentration in TZNYb glasses

The increase in density and packing-related properties with the addition of Yb_2O_3 signifies progressive glass densification. The incorporation of Yb^{3+} ions, which possesses a larger ionic radius of (176 pm) in comparison to Zn^{2+} ions (142 pm), results in the rearrangement of the glass network. Increases in Yb_2O_3

content result in the attainment of a more compact and rigid structure. This trend is directly influenced by the presence of Yb^{3+} ions. The Yb^{3+} ions concentration (N_{Yb3+}) increases from 0.1173 x 10^{21} to 0.6084 x 10^{21} ions cm^{-3}. It has been demonstrated that these variations specifically impact the polaron radius (r_p), the inter-ionic distance (r_i), and the field strength (F_S). The radius of the polaron and the inter-ionic distance both decrease from 7.434 to 1.434 Å and 2.8 to 0.5 Å, respectively. Meanwhile, the field strength undergoes an increase from 0.0054 to 0.1460 x 10^{15} cm^{-2}, signifying the establishment of more pronounced which local electric fields surrounding the Yb^{3+} ions.

The simultaneous increase in density and decrease in molar volume suggest enhanced network connectivity. These behaviors can be related to a reduction in non-bridging oxygen (*NBO*) and an increase in bridging oxygen (*BO*) linkages [31]. This hyphothesis is supported by the increasing V_p and *OPD* parameters. These results indicate a higher degree of network cross-linking [32]. The reduction in inter-ionic distance and polaron radius suggests a stronger Yb-O local field effect [33]. These present findings thus confirm that the incorporation of Yb_2O_3 has significant influence on both the physical and structural properties of the TeO_2-ZnO-Na_2O glass system.

3.2. Estimated mechanical properties

The mechanical properties of TZNYb glasses were estimated via the Makhisima-Mackenzie model. The calculated parameters are presented in Fig. 2. The total dissociation energy (G) increases slightly from 51.67 to 52.08 kJ cm^{-3} with increasing Yb_2O_3 content. This growth is indicative of the contribution of system constituents, namely oxides (TeO_2=54 kJ cm^{-3}), (ZnO=49.9 kJ cm^{-3}), and (Na_2O= 31.9 kJ cm^{-3}). The dissociation energy is directly related to the overall bond strength within the glass network.

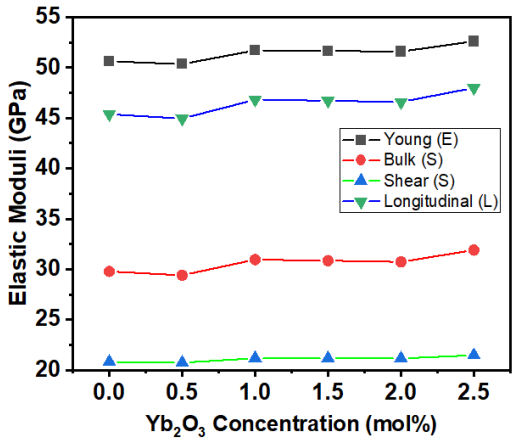

Fig. 2. Elastic moduli as a function of Yb_2O_3 concentration in TZNYb glasses

Consequently, all elastic moduli demonstrate systematic increases with Yb_2O_3 addition. Young's modulus increases from 50.66 to 52.61 GPa, while the bulk modulus rises from 29.77 to 31.89 GPa. Similarly, the shear modulus increases from 20.81 to 21.47 GPa, while the longitudinal modulus demonstrates an increase from 45.38 to 48 GPa. The enrichment of these moduli is indicative of increased rigidity and resistance to deformation. The obtained results suggest the presence of stronger inter-atomic bond and a higher degree of network cross-linking within the glass matrix [34].

The Poisson ratio remains within the range of 0.4298-0.4324 indicating that the overall deformation mechanism of the glass network is unaffected by Yb_2O_3 addition. Furthermore, an increase the microhardness parameter from 0.0158 to 0.0164 with increasing Yb_2O_3 concentration, thereby confirming a more compact and robust glass network [35].

3.3. Optical properties

The UV-Vis absorption spectra of TZNYb glasses were recorded in the range of 330-1050 nm. As illustrated in Fig. 3, a distinct absorption band is observed around 981 nm. The band that is characteristic of the $(^2F_{7/2}) \rightarrow (^2F_{5/2})$ electronic transition of Yb^{3+} ions, is distinctive band of ytterbium-doped glass systems [36]. As demonstrated in Fig. 4, position of the $(^2F_{5/2})$ absorption band remains unchanged with increasing of Yb_2O_3 concentration. This phenomenon under discussion can be understood in view of the shielding of 4f electrons by outer 5s and 5p orbitals. The observed absorption area increased significantly (74 to 323), and the full width at half maximum (FWHM) broadened from 19.38 to 43.74 nm.

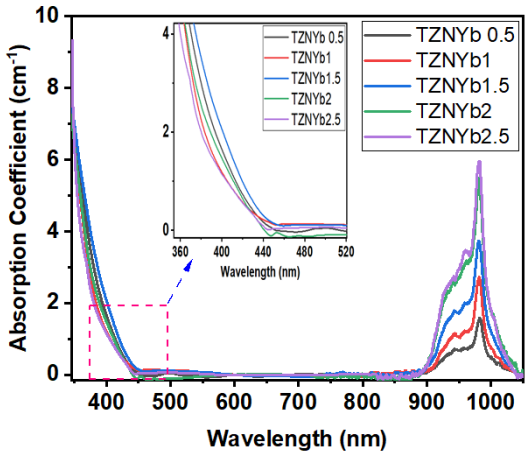

Fig. 3. UV-Vis absorption spectra of TZNYb glasses at different Yb_2O_3 concentration

Meanwhile, in the presence of lower Yb_2O_3 concentration (≤ 1.5 mol%), a shift in the UV absorption edge is observed towards longer wavelengths. This phenomenon is associated to the alteration in the formation of non-bridging oxygen (NBO). In the case of higher concentration (2.0-2.5 mol%), the absorption edge shifts towards the shorter wavelengths, possibly due to Yb^{3+} ions clustering and structural rearrangement of the glass network [37].

The optical band gap (E_g) was determined using Tauc plot analysis with the Davis-Mott model. The Tauc plot for the undoped sample (TZNYb0) is displayed in Fig. 5. The variation of E_g with Yb_2O_3 content is presented in Fig. 6. It is evident that the optical band gap increases from 3.01 eV to 3.30 eV with increasing Yb_2O_3 concentration. At lower concentration (≤ 1.5 mol%), a slight decrease in E_g is observed and attributed to the formation of NBOs linkages. At higher concentrations (2.0-2.5 mol%), increase in E_g suggests a more rigid and connected network [38].

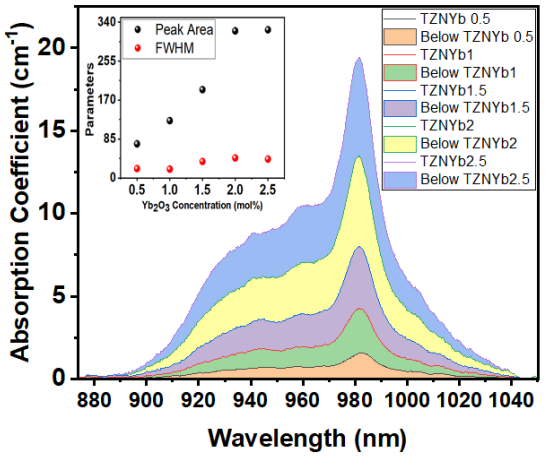

Fig. 4. Evolution of the Yb^{3+} absorption band (~980 nm), including integrated area and FWHM, as function of Yb_2O_3 concentration

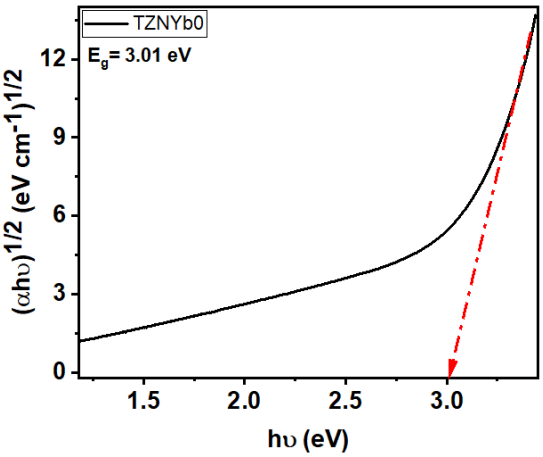

Fig. 5. Tauc plot ($\alpha h\nu^{1/2}$) versus hν of TZNYb0 glass

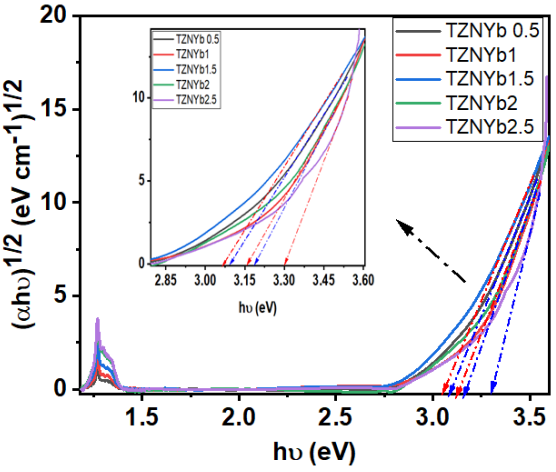

Fig. 6. Variation of optical band gap (E_g) with Yb_2O_3 concentration in TZNYb glasses

The refractive index was estimated using the Dimitrov-Sakka ($n_{D\text{-}S}$), Moss (n_M), and Kumar (n_R) models as illustrated in Fig. 7. All models consistently indicate a decrease in refractive index in proportion to the increase in Yb_2O_3 content. The average refractive index (n_v) also decreases systematically (Fig. 8), which is attributed to the reduction in *NBO* concentration, as *NBO*s exhibit higher electronic polarisability than *BO*s [39].

Other optical parameters, including molar refractivity (R_m) and electronic molar polarisability (α_m), decrease with increasing Yb_2O_3 content. R_m value decreases from 17.83 to 16.88, while α_m decreases from 7.073 x 10^{-24} to 6.695 x 10^{-24} cm^3. This indicate a reduction in the electronic polarizability of the glass network [40]. Reflection Loss (R_L) decreases from 0.1657 to 0.1559, while the transmittance coefficient (T) increases from 0.7143 to 0.7284, thereby demonstrating enhanced optical performance [41]. Meanwhile, the metallization criterion (M) calculated from the ratio V_m to R_m, ranges from 0.300 to 0.318, confirming the non-metallic nature of the investigated glass system.

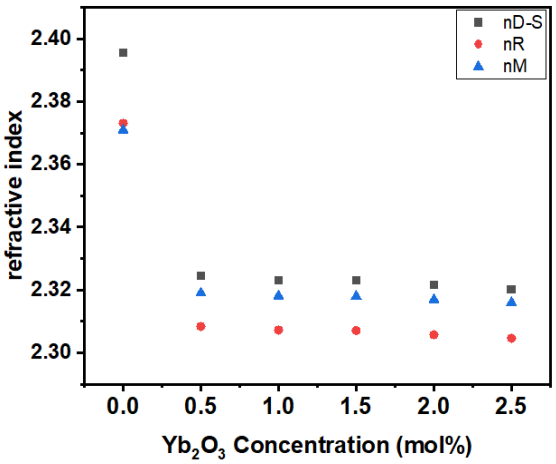

Fig. 7. Refractive index of TZNYb glasses estimated using Dimitrov-Sakka, Moss, and Kumar models

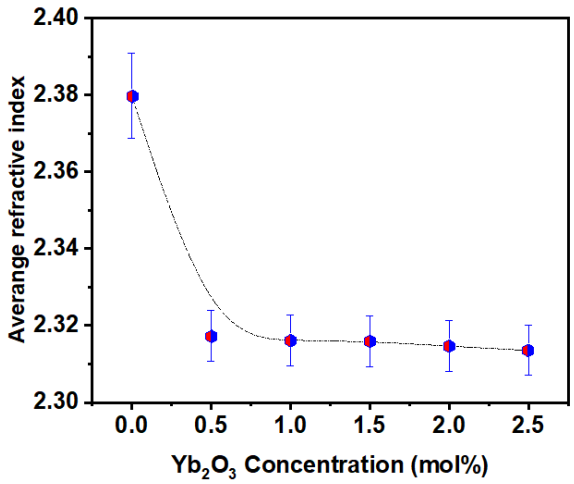

Fig. 8. Average refractive index (n_v) of TZN Yb glasses as function of Yb_2O_3 concentration

3.4. Infrared absorption analysis

The FTIR spectra of TZNYb glasses have been recorded in the range of 400-4000 cm^{-1} as illustrated in Fig. 9. The broad absorption bands observed at around 3400 and 1600 cm^{-1} are attributed to O-H stretching and bending vibrations, respectively [42]. A band around 400 cm^{-1} corresponds to Zn-O vibrations, indicating the role of ZnO as a network modifier [43]. A prominent absorption band around 660 cm^{-1} has been

observed to be associated with TeO_2 structural units.

Tellurite glass networks are constitued primarily of trigonal bipyramidal (tbp) TeO_4 units and trigonal pyramidal TeO_3 (tp) units [44]. The quantification of these units was achieved through the implementation of spectral deconvolution within the tellurite fingerprint region.

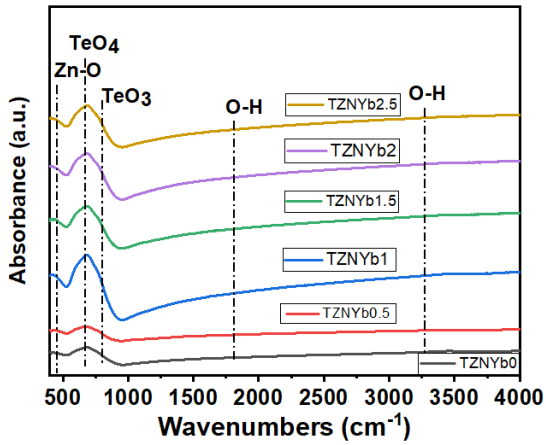

Fig. 9. FTIR spectra of TZNYb glasses in the range 400-4000 cm^{-1}

The deconvoluted spectra for TZNYb0 and TZNYb2.5 are presented in Fig. 10 and Fig. 11, with a fitting cofficient $R^2 \approx 0.999$. The peaks observed at 600 and 670 cm^{-1} are attributed to TeO_4 units, while the peak near 750 cm^{-1} is assigned to TeO_3 units. The relative fractions of TeO_4 (N_4) and TeO_3 (N_3) are demonstrated in Fig. 12. The N_4 value increases from 0.21 to 0.53, while N_3 decreases from 0.78 to 0.42 with increasing Yb_2O_3 content. This finding suggests that there has been a partial conversion of TeO_3 units to TeO_4 units, suggesting enhanced network polymerization. The structural evolution under consideration provides a theoretical basis for the optical findings, particularly the increase in band gap energy and decrease in the refractive index. These phenomena are associated with reduced electronic polarizability and increased network connectivity. The high field strength of Yb^{3+} ions has been demonstrated to promote local structural rearrangements, thereby modifying Te-O bonding configurations and influencing both vibrational and optical responses of the glass system [45].

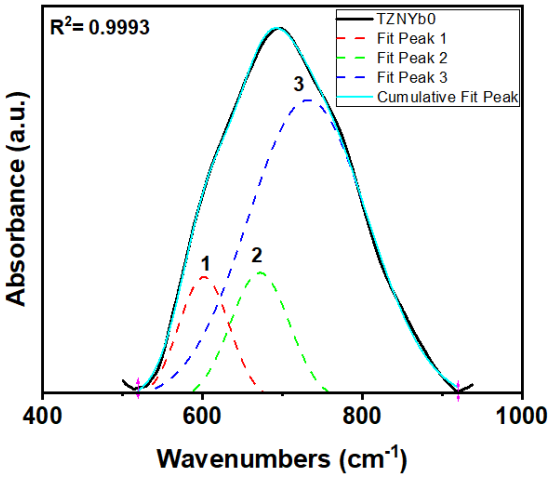

Fig. 10. Deconvolution on tellurite fingerprint region for TZNYb0 glass

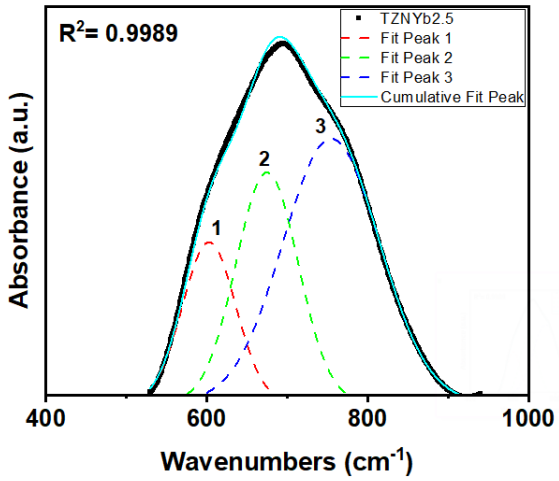

Fig. 11. Deconvolution on tellurite fingerprint region for TZNYb2.5 glass

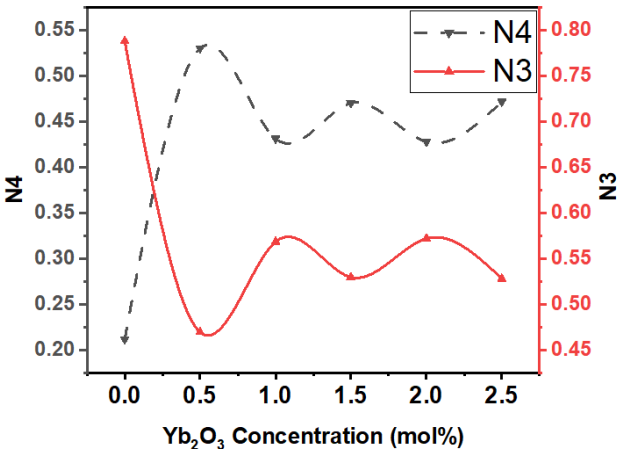

Fig. 12. Variation of TeO_4 (N_4) and TeO_3 (N_3) fractions as function of Yb_2O_3 concentration

4. Conclusion

The fabrication of Ytterbium-doped TeO_2-ZnO-Na_2O (TZNYb) glasses with a variation of 0-2.5mol% Yb_2O_3 was successfully achieved via the melt-quenching technique. An examination was conducted to ascertain the physical, mechanical, and optical properties of the subject. The incorporation of Yb^{3+} ions has been demonstrated to induce glass network densification. It is evidenced by increased density, reduced molar volume, and enhanced glass packing density. This structural transformation has been shown to enhance mechanical rigidity by increase in glass elastic moduli (E, B, S, and L). In terms of optical properties, the addition of Yb_2O_3 results in a widening of the optical band gap and decrease in both the refractive index and the reflection loss. This phenomenon can be suggested due to the reduction of glass polarizability. Meanwhile, FTIR analysis confirms a shift from TeO_3 to TeO_4 structural units in view of decrease in NBO linkages, which suggest increased glass network connectivity. The results demonstrate that low-level Yb_2O_3 incorporation has the capacity to tailor the structural, mechanical, and optical properties of TZN glasses. The potential of these elements is unlocked in photonic applications such as particularly in solid-state lasers, optical amplifiers, and spectral converters.

Acknowledgements

The authors acknowledged with gratitude to Ministry of Higher Education, Science, and Technology of the Republic of Indonesia for the financial support to carry out this work with Contract of Research Grant: 105/C3/DT.05.00/PL/2025.

References

1. N. Boudchicha, M. Iezid, F. Goumeidane, M. Legouera, P. S. Prasad, and P. V. Rao, *Judd–Ofelt Analysis and Spectroscopy Study of Tellurite Glasses Doped with Rare-Earth (Nd^{3+}, Sm^{3+}, Dy^{3+}, and Er^{3+})*. Mater. 16 (2023) 6832
2. B. Srinivas, K. M. Katubi, A. Bhogi, S. Ahamed, T. V. Surendra, A. Hameed et al., *Synthesis, optical, and spectroscopic studies of bismuth boro-tellurite glass system containing BaO and V_2O_5*, Opt. Quantum Electron. 56 (2024) 5
3. B. Bureau, S. Danto, H. L. Ma, C. Boussard-Plédel, X. H. Zhang, and J. Lucas, *Tellurium based glasses: A ruthless glass to crystal competition*, Solid State Sci. 10 (2008) 427–433
4. H. A. A. Sidek, S. Rosmawati, Z. A. Talib, M. K. Halimah, and W. M. Daud, *Synthesis and Optical Properties of ZnO-TeO2 Glass System*, Am. J. Appl. Sci. 6 (2009) 1489–1494
5. S. Blanchandin, P. Marchet, P. Thomas, J. C. Champarnaud-Mesjard, B. Frit, and A. Chagraoui, *New investigations within the TeO_2-WO_3 system: phase equilibrium diagram and glass crystallization.* J. Mater. Sci. 34 (1999) 4285–4292
6. W. Widanarto, M. R. Sahar, S. K. Shoshal, R. Arifin, and M. S. Rohani, *Optical and Magnetic Properties of TeO_2·ZnO·Li_2O glass system containing natural Fe_3O_4 particles,* Ber. Fis. 16 (2013) 95-102
7. K. Linganna, J.-H. In, S. H. Kim, K. Han, and J. H. Choi, *Engineering of TeO_2-ZnO-BaO-Based Glasses for Mid-Infrared Transmitting Optics*, Mater. 13 (2020) 5829
8. A. Marzuki and D. E. Fausta, *Effect of TiO_2 Addition on Optical Properties of TeO_2-ZnO-PbO Glasses*, IOP Conf. Ser.: Mater. Sci. Eng.858 (2020) pp. 012035
9. J. Massera, J. Remond, J. Musgraves, M. J. Davis, S. Misture, L. Petit et al., *Nucleation and growth behavior of glasses in the TeO_2–Bi_2O_3–ZnO glass system*, J. Non-Cryst. Solids. 356 (2010) 2947–2955
10. N. B. Mohamed, T. F. S. T. Shahrir, & S. N. M. Rafien, *Structural and Physical Properties of TeO_2-B_2O_3-ZnO Glasses: Evidence of the Mixed-Glass-Former Effect*. Solid. State. Sci. 33 (2025) 97-107
11. J. de Clermont-Gallerande, S. Saito, M. Colas, P. Thomas, and T. Hayakawa, *New understanding of TeO_2–ZnO–Na_2O ternary glass system*, J. Alloys Compd., 854 (2021) 157072
12. S. K. Ghosal, A. Awang, M. R. Sahar, R. J. Amjad, M. R. Dousti, *Spectroscopic and structural properties of TeO_2-ZnO-Na_2O-Er_2O_3-Au glasses*. Chalcogenide Lett. 10 (2013) 411-420
13. S. Badamasi & Y.A. Tanko. *Thermal Properties of TeO_2-ZnO-Na_2O Glasses: Effect of Dy_2O_3 Doping*. Sci. World J.. 13 (2018)
14. E. J. Voss, J. Ruiz, and M. Vendetti, *Preparation and characterization of TeO_2-ZnO-Na_2O glasses doped with Eu_2O_3*, ACS. (2020).
15. J. Y. Mirdda, S. Mukhopadhyay, K. R. Sahu, & M. N. Goswami, *Optical and Electrical Properties of Nd^{3+}doped Na_2O-ZnO-TeO_2 Material*. Biointerface Res Appl Chem. 12 (2021) 7927–7941
16. S. Shen, A. Jha, E. Zhang, and S. J. Wilson, *Compositional effects and spectroscopy of rare earths (Er^{3+}, Tm^{3+}, and Nd^{3+}) in tellurite glasses*, C. R. Chim. 5 (2002) 921–938
17. A. N. Rahmawati, A. Marzuki, V. Suryanti, A. M. Indryani, D. E. Fausta, F. A. Alvyanti et al., *Absorption Spectra Analysis of Nd/Yb Codoped Boro-Tellurite Glasses*, KEM. 993 (2024) 17–24
18. M. A. Merzliakov, V. V. Kouhar, G. E. Malashkevich, and E. V. Pestryakov, *Spectroscopy of Yb-doped tungsten–tellurite glass and assessment of its lasing properties*. Opt. Mater. 75 (2018) 142–149
19. J. S. Alzahrani, A. Hammoud, I. Boukhris, Z. A. Alrowaili, A. V. Lebedev, I. O. Olarinoye, M. S. Al-Buriahi, *Fabrication and characterization of TeO_2–Na_2O–BaO glass doped with Yb_2O_3 for optical and particulate-radiation shielding applications: Role of Bi_2O_3/WO_3,* Opt. Mat.. 150 (2024) 115141
20. S.-B. Lin, P. Fang, J. She, H T. Guo, S-N. Xu, et al., *Spectroscopic and thermal properties of novel Yb^{3+}-doped TeO_2–PbO–Nb_2O_5 based tellurite glasses with high emission cross-section*. Mod. Phys. Lett. B. 28 (2014) 1450198
21. S. Ariyanti, A. Marzuki, Cari, A. H. Ramelan, D. E. Fausta, Harjana, & A. D. Sutomo, Physical Properties Investigation of Bi_2O_3-PbO-B_2O_3-P_2O_5 Glasses, J. Phys.: Conf. Ser. 2945 pp. 012006
22. A. Marzuki, H. Purwanto, A. D. Sutomo, Harjana, A. H. Ramelan, D. E. Fausta et al. *Physical Properties Study of Sodium Doped Boro-Tellurite (Na_2O: TeO_2-B_2O_3-ZnO) Glasses,* MSF. 1118 (2024) 3–10
23. M. A. Algradee, M. Sultan, O. M. Samir, and A. E. B. Alwany, *Electronic polarizability, optical basicity and interaction parameter for Nd_2O_3 doped lithium–zinc–phosphate glasses,* Appl. Phys. A. 123 (2017)
24. W. M. S. Djeksadipura, A. Marzuki, D. E. Fausta, and V. Suryanti, *Structural Properties of Tm_2O_3/Ho_2O_3 Co-Doped Borotellurite Glass Analyzed Using FTIR.* Glass Phys. Chem. 51 (2025) 34–47
25. I. V. G. Amaya et al., *Effect of CdO on the Structural and Spectroscopic Properties of Germanium–Tellurite Glass,* Mater. 18 (2025) 1739
26. A. A. Ahmed and S. Q. Mawlud, *Physical and optical properties of ternary lead-bismuth tellurite glass*, Heliyon. 9 (2023). e16730
27. A. Marzuki, V. Suryanti, R. Suryana, Harjana, R. W. Astuti, D. E. Fausta et al., *Mechanical properties of lead borate glass doped neodymium,* AIP Conf. Proc. 3166 (2025) pp. 020039
28. A. Marzuki, W. M. S. Djeksadipura, V. Suryanti, D. E. Fausta, A. Saraswati, and G. T. Singgih, Compositional dependence of density and refractive index in borotellurite glass, J. Phys.: Conf. Ser. 1912 (2021) pp. 012026
29. G. Venkataiah, P. Babu, I. R. Martin, K. V. Krishnaiah, K. Suresh, V. Lavin et al., *Spectroscopic studies on Yb3+-doped tungsten-tellurite glasses for laser applications,* J. Non-Cryst. Solids 479 (2018) 9–15
30. S. Inaba, S. Fujino, and K. Morinaga, *Young's Modulus and Compositional Parameters of Oxide Glasses,* J. Am. Ceram. Soc. 82 (1999) 3501–3507
31. F. A. Abdel-Wahab, A. M. Fayad, M. Abdel-Baki, and H. AbdelMaksoud, *Role of non-bridging oxygen defect in the ionic conductivity and associated oxygen trap centers in lead-borate oxide glass: Effect of structural substitution of PbO for Ag_2O and Li_2O modifiers*, J. Non-Cryst. Solids. 500 (2018) 84–91,
32. N. M. Reddy, *Effect of Rare Earth Ions Doping on Glass Materials,* Mater. Sci. IntechOpen, (2025).
33. N. T. El-Shamy, E. M. Mahrous, S. K. Alghamdi, M. J. Tommalieh, M. H. Nasr, H. M. Abomostafa et al., *The influence of ytterbium oxide (Yb_2O_3) substitution in cadmium bismuth borate glasses: An approach to improve structural, optical, and radiation shielding efficiency,* Ceram. Int. 51 (2025) 6319–6329
34. A. Moghanian, A. Pazhouheshgar, & A. Rajabpour, *Correlating between atomic structure and mechanical properties in cobalt-doped silicate glasses via molecular dynamics and machine learning,* Results Eng. 30 (2026) 110575
35. S. B. Adamu, M. K. Halimah, K. T. Chan, F. D. Muhammad, S. N. Nazrin, E. Scavino et al., *Structural, prediction and simulation of elastic properties*

for tellurite based glass systems doped with nano and micro Eu_2O_3 particles via artificial neural network model, J. Mater. Res. Technol. 17 (2022) 586–600

36. Z. Zhao, B. Zhang, Y. Gong, Y. Ren, M. Huo, and Y. Wang, *Concentration effect of Yb3+ ions on the spectroscopic properties of high-concentration Er^{3+}/Yb^{3+} co-doped phosphate glasses*, J. Mol. Struct. 1216 (2020) 128322
37. G. Kilic et al., *Ytterbium (III) oxide reinforced novel TeO_2–B_2O_3–V_2O_5 glass system: Synthesis and optical, structural, physical and thermal properties,* Ceram. Int. 47 (2021) 18517–18531
38. S. F. Hathot, B. M. Al Dabbagh, and H. Aboud, *Structural and spectroscopic correlation in barium-boro-tellurite glass hosts: effects of Dy_2O_3 doping*, Chalcogenide Lett. 21 (2024) 201–215
39. N. Elkhoshkhany, S. Marzouk, M. El-Sherbiny, S. Yousri, M. S. Alqahtani, H. Algarni et al., *Enhanced thermal stability and optical and structural properties of Tm^{3+} ions in doped tellurite glasses for photonic use*, Results Phys. 24, (2021) 104202
40. M. K. Halimah, M. F. Faznny, M. N. Azlan, and H. A. A. Sidek, *Optical basicity and electronic polarizability of zinc borotellurite glass doped La^{3+} ions*, Results Phys. 7 (2017) 581–589s
41. S. A. Umar, M. K. Halimah, K. T. Chan, and A. A. Latif, *Polarizability, optical basicity and electric susceptibility of Er^{3+} doped silicate borotellurite glasses*, J. Non-Cryst. Solids. 471 (2017) 101–109
42. S. H. Alazoumi, S. A. Aziz, R. El-Mallawany, U. S. Aliyu, H. M. Kamari, M. H. M. M. Zaid et al., *Optical properties of zinc lead tellurite glasses*, Results in Physics, 9. (2018) 1371–1376
43. D. E. Fausta, A. Marzuki, and Cari, Infrared absorption spectra analysis of TeO_2-ZnO-Bi_2O_3-TiO_2 doped B_2O_3 glasses, J. Phys.: Conf. Ser. 1511 (2020) pp. 012076
44. J. N. Ayuni, M. K. Halimah, Z. A. Talib, H. A. A. Sidek, W. M. Daud, A. W. Zaidan, & A. M. Khamirul, Optical Properties of Ternary TeO_2-B_2O_3-ZnO Glass System, IOP Conf. Ser.: Mater. Sci. Eng. 17 (2011) pp. 012027
45. J. de Clermont-Gallerande, S. Saito, T. Hayakawa, M. Colas, J-R. Duclere, & P. Thomas, *Optical properties of Nd^{3+}-doped TeO_2-TiO_2-ZnO glasses with lower hydroxyl content*, J. Non-Cryst. Solids. 528 (2020) 119678.